



HAL
open science

Infiltration of nickel and copper catalysts into a GDC backbone assisted by supercritical CO₂ for efficient SOFC anodes

Laura Guesnet, Guillaume Aubert, Hubert S., Pierre-Marie Geffroy, Cyril Aymonier, Jean-Marc. Bassat

► **To cite this version:**

Laura Guesnet, Guillaume Aubert, Hubert S., Pierre-Marie Geffroy, Cyril Aymonier, et al.. Infiltration of nickel and copper catalysts into a GDC backbone assisted by supercritical CO₂ for efficient SOFC anodes. *Sustainable Energy & Fuels*, 2022, 6 (7), pp.1801-1811. 10.1039/D2SE00251E . hal-03618300

HAL Id: hal-03618300

<https://hal.science/hal-03618300>

Submitted on 24 Mar 2022

HAL is a multi-disciplinary open access archive for the deposit and dissemination of scientific research documents, whether they are published or not. The documents may come from teaching and research institutions in France or abroad, or from public or private research centers.

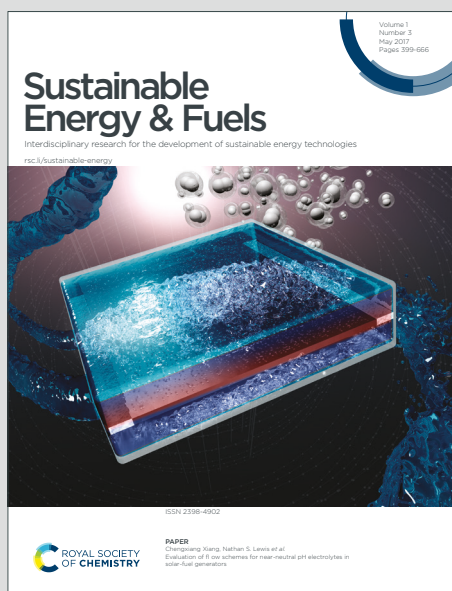
L'archive ouverte pluridisciplinaire **HAL**, est destinée au dépôt et à la diffusion de documents scientifiques de niveau recherche, publiés ou non, émanant des établissements d'enseignement et de recherche français ou étrangers, des laboratoires publics ou privés.

Sustainable Energy & Fuels

Interdisciplinary research for the development of sustainable energy technologies

Accepted Manuscript

This article can be cited before page numbers have been issued, to do this please use: L. Guesnet, G. Aubert, S. Hubert, P. Geffroy, C. Aymonier and J. Bassat, *Sustainable Energy Fuels*, 2022, DOI: 10.1039/D2SE00251E.



This is an Accepted Manuscript, which has been through the Royal Society of Chemistry peer review process and has been accepted for publication.

Accepted Manuscripts are published online shortly after acceptance, before technical editing, formatting and proof reading. Using this free service, authors can make their results available to the community, in citable form, before we publish the edited article. We will replace this Accepted Manuscript with the edited and formatted Advance Article as soon as it is available.

You can find more information about Accepted Manuscripts in the [Information for Authors](#).

Please note that technical editing may introduce minor changes to the text and/or graphics, which may alter content. The journal's standard [Terms & Conditions](#) and the [Ethical guidelines](#) still apply. In no event shall the Royal Society of Chemistry be held responsible for any errors or omissions in this Accepted Manuscript or any consequences arising from the use of any information it contains.

Infiltration of nickel and copper catalysts in a GDC backbone assisted by supercritical CO₂ for efficient SOFC anodes

View Article Online
DOI: 10.1039/D2SE00251E

L. Guesnet^{1,2}, G. Aubert¹, S. Hubert¹, P.M. Geffroy²,
C. Aymonier¹ and J.M. Bassat^{1,*}

¹ CNRS, Univ. Bordeaux, Bordeaux INP, ICMCB, UMR 5026, F-33600 PESSAC Cedex, France

² CNRS, Institut de Recherche sur les Céramiques (IRCER), UMR 7315, Centre Européen de la Céramique, 12 rue Atlantis, 87068 LIMOGES Cedex, France

*Corresponding author. Tel: +33(5)40002753; fax: +33(5)40002761; e-mail address: jean-marc.bassat@icmcb.cnrs.fr

Abstract

This study describes an original method developed for the shaping of composites Solid Oxide Fuel Cells (SOFC) anodes including either nickel or copper as metal. There are prepared by catalyst (nickel or copper nitrates) infiltration in a porous GDC (Ce_{0.9}Gd_{0.1}O_{1.95}) skeleton. The infiltration by classical way is compared to the original infiltration by *supercritical way*. Therefore, this article details the difference between these two kinds of infiltration and will explain how the infiltration using supercritical CO₂ can finally lead to improve the electrochemical performances of the corresponding cells.

Keywords: SOFC, hydrogen electrodes, infiltration, supercritical fluids, nickel, copper

1. Introduction

View Article Online
DOI: 10.1039/D2SE00251E

During the recent years, Solid Oxide Cells (SOC) operating at high or intermediate temperatures have attracted more and more attention [1]. Indeed, their efficiency is high for the chemical energy conversion (SOFC - Solid Oxide Fuel Cell mode) as well as for the gas production (for instance, hydrogen and oxygen) when using available electricity in SOEC (Solid Oxide Electrolysis Cell) mode [2, 3]. The development of reversible devices is currently under investigation. Such devices do not produce greenhouse gases, which is of particular interest in the current environmental context and, more precisely in order to use renewable energy. For instance, when coupled to solar panels, SOEC can produce « green » hydrogen [4, 5].

For the SOC commercialization, the main challenge concerns the reduction of the operating temperature, which is currently too high (800-1000°C). A direct consequence of the high operating temperature is a decrease of the lifetime of the cell and correspondingly the cost is still too high. Then one of the main goal is to operate the cell at lower temperatures, typically 500-600°C [6, 7]. Among others, the degradation of the cell at high temperature generally arises from an electrode microstructure alteration (grain coarsening, segregation, as well as a chemical reactivity between the electrolyte and the electrodes [8–12]), especially on the hydrogen side.

Even if alternative oxides are also developed, the material generally used as fuel electrode is a Ni-YSZ (yttria stabilized zirconia) cermet, the electronic conductivity being ensured by the nickel network, while the ionic conductivity of the electrode occurs among the percolating YSZ grains. This composite is chosen because of its stability under hydrogen at high temperature and its high catalytic activity [13–15].

Conventional (thick) Ni/YSZ cermets are mostly shaped by tape-casting. Commercial NiO and YSZ powders are ball - milled until obtaining a homogeneous mixture. In a second step, organic additives (solvent, binder, dispersed agent, plasticizer) are added to the powder in order to get a slurry. This one is casted to obtain a self-supported green tape after solvent removal [2, 16, 17]. The issues usually encountered are both segregation and evaporation of nickel [13, 14]. In particular, the nickel grain agglomeration is increased under electrical polarization and a significant increase of the mean Ni particle diameter is evidenced [3]. It is well known that at high temperature (800-1000°C), the nickel has a high surface mobility, causing sintering and grain growth [20]. Unfortunately, the Ni coarsening is responsible of an electrode performance loss (18 to 41 % of the total performance degradation is due to the nickel coarsening) [21]. When the nickel agglomerates, the percolation of these metallic particles decreases; this is the same for the TPB (Triple Phase Boundaries) density [22]. The second observed phenomenon is the nickel evaporation in its hydroxide form Ni(OH)₂ (volatile particles) by diffusion through the cermet porosity [18].

Therefore, changing the initial microstructure as well as decreasing the operating temperature are two ways limiting the degradation phenomena of the electrode [20, 21, 23]. At the microstructure level, the cell performance can be improved by enhancing the TPB site number, *i.e.* when increasing the electrode surface [24]. Therefore, the catalyst impregnation into a porous ionic conducting skeleton is an adequate preparation method for the electrode shaping, because it permits to sinter the electrode at low temperature, and to increase the reaction area offered by the nanoparticle size of the final deposited oxides. With this method, only the porous backbone (same nature than the electrolyte) is sintered at high temperature, and the catalyst is annealed at low temperature, which allow limiting the reactivity phenomena [20 – 24].

Recently, the infiltration of nickel (or other elements) into a porous YSZ or GDC backbones was performed, and the electrochemical performance improved [18, 25 – 28]. Indeed, when infiltrating an electronic conductor into a porous ionic conductor, the hydrogen oxidation reaction is delocalized over the whole surface of the electrode, thus increasing the TPB site number [27, 29 – 33]. There is a real interest to think about innovative infiltration methods such as that assisted by supercritical carbon dioxide.

Indeed, supercritical fluids exhibit interesting properties as gas-like viscosity, liquid-like density and diffusion coefficients higher than that of liquids. Supercritical fluids (SCFs) permit to produce a large variety of functional materials [39], which could be used in different domains of application: battery, polymers, sensors, optics, fuels cells etc. Among the supercritical fluids-based methods to prepare materials, the supercritical fluid chemical deposition (SFCD) can be used to incorporate metallic nanoparticles into porous supports; SFCD has been used for instance to synthesize electrocatalysts in the case of proton exchange membrane fuel cells (PEMFC) at low temperature [40]. This impregnation technique permits to get nanoparticle sizes. Likewise, the supercritical fluid utilization is environmentally-friendly (without degradation and contamination) and it is also a fast and efficient technique to infiltrate porous supports [41]. Nevertheless, nothing was still developed regarding the impregnation of supports for SOC applications.

In this context, this article reports an efficient anode shaping method based on the infiltration of a catalyst precursor (nickel or copper nitrates) into a porous GDC10 ($\text{Ce}_{0.9}\text{Gd}_{0.1}\text{O}_{2-\delta}$) skeleton assisted by supercritical carbon dioxide. The infiltration assisted by supercritical carbon dioxide is compared to the conventional infiltration. The results regarding both the microstructure and the electrochemical performance are detailed and discussed.

2. Experimental

View Article Online
DOI: 10.1039/D2SE00251E

2.1. Shaping of electrolyte/backbone/collecting layer

The electrolyte was prepared using gadolinium doped ceria GDC10 ($\text{Ce}_{0.9}\text{Gd}_{0.1}\text{O}_{2-\delta}$), here chosen because of its high ionic conductivity at reduced temperature ($\sigma_i = 0.02 \text{ S.cm}^{-1}$ at 600°C). A commercial GDC10 powder with an average diameter of $0.25 \mu\text{m}$ was provided by Solvay company. The powder was first uniaxially pressed at 200 bar to prepare a green pellet as support, with 25 mm and 9 mm in diameter and thickness, respectively. To obtain dense pellets (with a relative density larger than 95 %), the samples were conventionally sintered at 1500°C during 3 h in air in a tubular furnace. The pellet dimensions after sintering were 19 mm and 8 mm in diameter and thickness, respectively. Afterwards, a symmetrical GDC10 porous skeleton and a symmetrical collecting layer of nickel oxide were deposited on the electrolyte by screen-printing [31]. The diameter of these two layers is decreased from 19 mm (pellet dimension) down to 16 mm to avoid any short-circuit. The GDC10 backbone and the collecting layer thicknesses were $30 \mu\text{m}$ and $10 \mu\text{m}$, respectively. Then, the obtained scaffold was annealed at 1150°C during 1 h under air. This architecture is shown on the Figure below (Figure 1). After sintering, the backbone porosity is around 45 % as already detailed in our own reference [42], permitting the catalyst infiltration. In the next future we aim to estimate more accurately the pore morphology, *i.e.* the amount of closed and open pores, in particular.

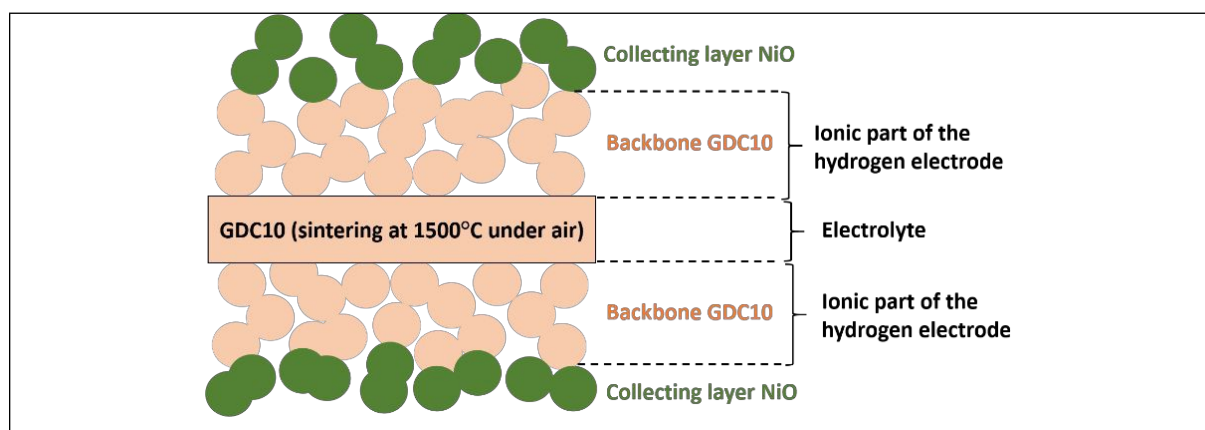


Figure 1. Scheme of a symmetrical hydrogen electrode before catalyst infiltration

2.2. Catalyst precursor infiltration

2.2.1) Conventional infiltration method

In a second step, the catalyst precursor was infiltrated in one step at the same time in the backbone and the collecting layer [36 – 38]. Two catalyst precursors were chosen: nickel and copper nitrates. A concentrated solution of nickel (copper) nitrate was infiltrated several times until the mass ratio of the

infiltrated material over the backbone one reaches about 60 wt. % before reduction under hydrogen (to replicate the metal amount in Ni-GDC or Cu-GDC cermets). For this purpose, a drop of the solution was deposited on the sample, then let a couple of minutes under primary vacuum to facilitate the infiltration of the solution till the heart of the backbone. The cell was wiped with paper to remove the excess. Therefore, a large part of the deposited mass is unfortunately lost using this process (4 wt. % is infiltrated during one infiltration cycle instead of approximately 15 wt. %, which is the maximum that could be infiltrated from the deposited droplet). Hence, the utilization of supercritical carbon dioxide could be a solution to avoid this matter lost. The infiltrated samples were finally annealed at 450°C during 20 min to remove nitrates. NiO and CuO were obtained after annealing in air as expected and checked by XRD. In a last step, the symmetrical hydrogen cells were annealed at 600 °C, under H₂/3%H₂O gas flow to obtain the desired metal catalysts: metallic nickel or copper.

2.2.2) Infiltration assisted by supercritical CO₂

In parallel, a second and more innovative (at least regarding this application) infiltration way was developed in this publication: the infiltration assisted by supercritical carbon dioxide (scCO₂). Here, scCO₂ is used as a diffusion solvent of a solution into the porous skeleton. ScCO₂ was chosen because it is non-polluting, abundant, inexpensive, non-flammable and its critical coordinates can be easily reached (T_c = 31 ° C and P_c = 7.38 MPa) [46]. ScCO₂ has a low viscosity and high diffusivity, then it can easily enter inside such highly porous structures [33]. The solubility of a solute in a supercritical fluid is adjustable by modifying the fluid density through pressure for example; by depressurizing CO₂, the CO₂ density will decrease and consequently, the catalyst precursor will precipitate into the pores.

The sample was, first, infiltrated according to the classical infiltration route previously described, before being positioned in the high pressure reactor (Figure 2). The CO₂ was filled in a preheater (p ≈ 6 Mpa at 25°C), then heated up to 200°C to reach the supercritical conditions (the reached pressure is 140 bar). The reactor was positioned in a hot water bath (50°C) to keep a supercritical temperature. The valve after the preheater is opened in order to fill the reactor with preheated CO₂. The pressure in the reactor is regulated by a back pressure regulator (BPR) at 100 bar. Then, the CO₂ is in continuous flux during 30 minutes to dry the solvent.

Then, the samples were annealed at 450°C during 20 min to remove the nitrates. The nitrate solution was infiltrated by supercritical way several times to obtain the same oxide quantity than in the case of classical infiltration (60 wt. %). Finally, the symmetrical hydrogen cells were annealed at 600 °C, under H₂/3%H₂O gas flow to obtain the desired metal catalysts.

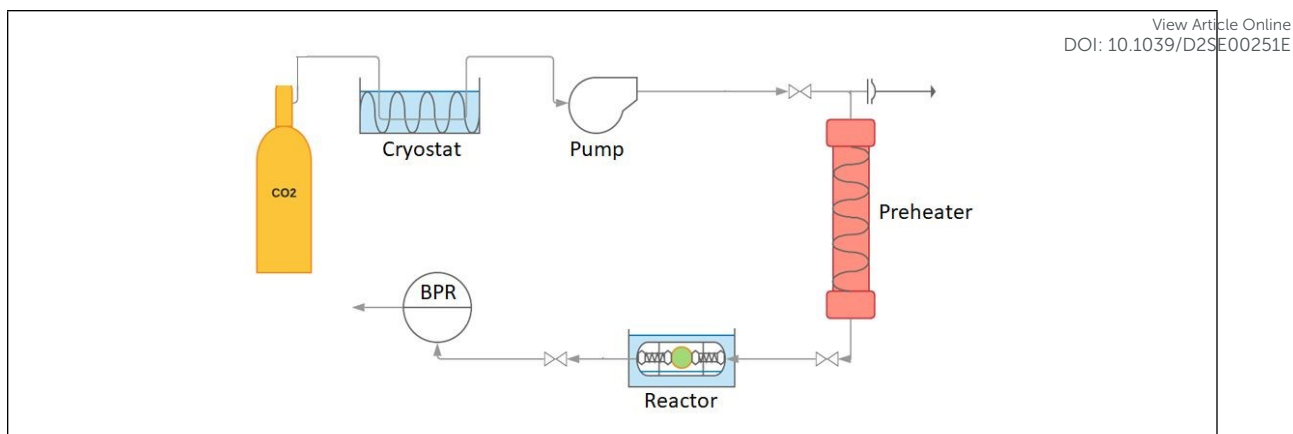


Figure 2. Schematic diagram of the full device used to infiltrate the SOFC electrodes assisted by scCO₂ treatment

2.3. Physicochemical and electrochemical characterizations

Two main characterization techniques of the infiltrated symmetrical cells were involved in this work:

- SEM images of each sample were recorded using a SEM-FEG HR (JEOL 6700F). High resolution images were obtained, while EDX leads to record mapping of sample area to evaluate the infiltration homogeneity. The samples were fractured and the images were recorded along the cross section. Before the analysis, the samples were coated with palladium/gold plasma to avoid any charge issue.
- The electrical resistances of the symmetrical cells were determined by impedance spectroscopy with the help of a Solartron Modulab. The symmetrical cells were placed between two gold grids supported by alumina ceramics; a weight was applied to improve the current collection. The impedance diagrams were recorded under H₂/3%H₂O each 50 °C between 400 °C and 600 °C in the frequency range 0.1 Hz – 1 MHz. The data were drawn using the Zview software. From the experimental data the two series and polarization resistances R_s and R_p were determined as detailed below.

The series resistance R_s mainly characterizes the ionic conductivity of the electrolyte σ_i, according to the relation (1):

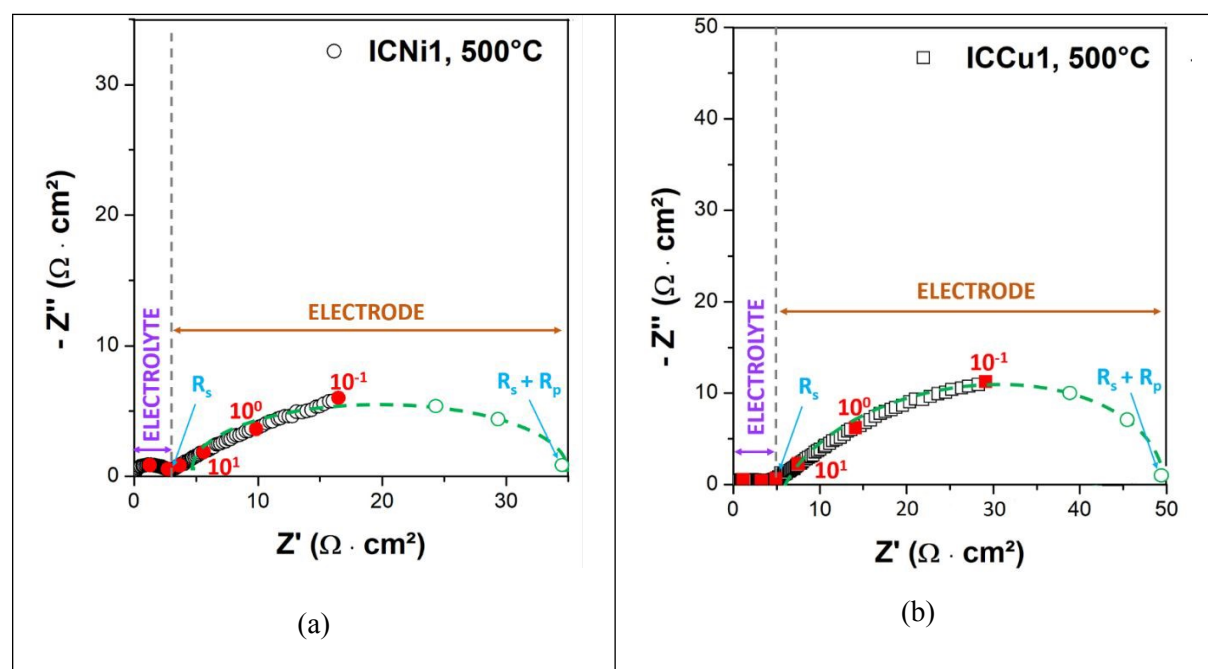
$$R_s = \frac{1}{\sigma_i} \cdot \frac{e}{S} \quad (1)$$

In addition to the O²⁻ ions migration, the resistance series also includes a (normally very small) part corresponding to the electrons migration in the electrode, as well as a the resistance of the interfaces between the different parts of the symmetrical cells (electronic or MIEC / ionic conductors for instance). In this work, the experimental R_s (Figure 3) was compared to that determined on a reference cell (R_{s ref}), *i.e.* a dense GDC10 pellet coated with platinum. The goal is to obtain a R_s value equal or possibly below R_{s ref} in order to prepare a infiltrated electrode (the composite GDC10 /Ni(Cu) with i) a sufficient

electronic conductivity level, ii) for which the resistance of the interfaces is minimized. For this purpose, the evolution of the ratio $\Delta R_s (R_s - R_{s \text{ ref}}) / R_{s \text{ ref}}$ versus temperature was plotted and discussed. The R_s value was easily determined, from an experimental point of view, by the interception of the diagram with the real axis (see Figure 3 for example).

In addition, the R_p resistance characterizes the electrode efficiency with respect to the involved reactions, on the hydrogen side in our study. The sum of the series and polarization resistances (R_s and R_p , respectively) were calculated from the impedance diagrams fitted using an equivalent circuit made of a series resistance and R-CPE equivalent elements. In some cases the experimental cycle ($R_s + R_p$) do not cross the real axis (see Figure 3.a as an example) and we used the fit to determine properly the required sum, then the R_p value itself after the subtraction of R_s . Obviously this procedure gives rise to a (limited, however) uncertainty of the absolute R_p value.

Figure 3 shows some examples of impedance diagrams recorded at 500°C plotted in Nyquist form. At this temperature, two semi-circles corresponding to the electrolyte (left semi-circle) and electrode (right semi-circle) are obtained. The empty green circles were estimated values, and they permitted to obtain the intercept between the semi-circle and the real axis. Each semi-circle intercept with the real axis permits to determine i) the series resistance (left extremity of the electrode semi-circle) and ii) the sum $R_s + R_p$ (right extremity of the electrode semi-circle). The whole experimental results will be gathered and discussed in the next section.



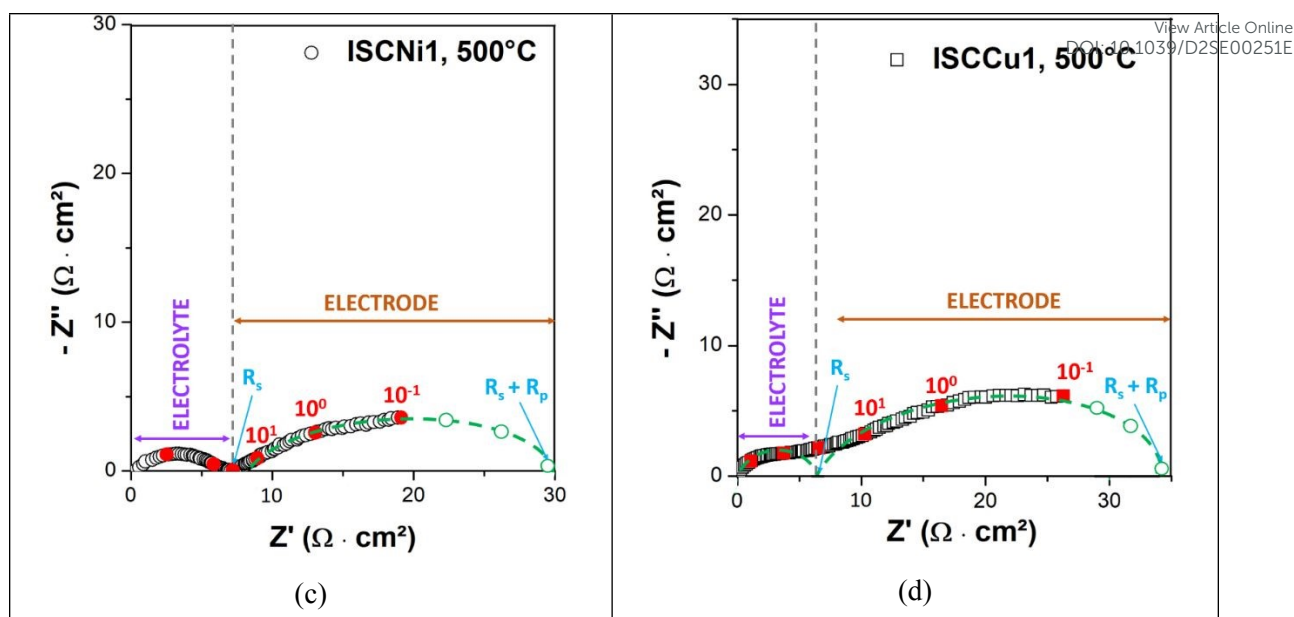


Figure 3. Example of impedance diagrams (Nyquist plot) recorded at 500°C on symmetrical half-cells (evolution of the imaginary part of the impedance as a function of its real part) with each frequency (red filled circles or squares) : (a) Classical Nickel infiltration (ICNi1), (b) : Classical Copper infiltration (ICCu1), (c) Supercritical Nickel infiltration (ISCNi1) and (d) : Supercritical Copper infiltration (ISCCu1). The diagrams are normalized with a thickness of 0,1 cm and fitted with an equivalent circuit.

3. Results and discussion

We aimed to improve the infiltration process, *i.e.* to decrease the infiltration cycles number by using supercritical CO₂.

So, in this part, the following experiments were performed :

- Classical and supercritical infiltration of nickel,
- Classical and supercritical infiltration of copper.

In the case of the classical infiltration route, the catalyst amount was modified in a previous work (between 30 and 70%), and the best result was obtained when using 60% of infiltrated catalyst, both for nickel and copper. It corresponds to the metal amount used in the usual cermet Ni(Cu)-GDC, and 15 cycles were involved to reach this metal amount. For the supercritical infiltration route, the infiltration rate was then fixed at 60%, and our purpose was to vary the experimental conditions of the infiltration (nature of the solvent, process of the infiltration, as detailed below).

Table 1 sums up the results obtained after the infiltration steps regarding the material characteristics *via* XRD and SEM/EDX measurements.

Table 1. Main characteristics of the used catalysts

View Article Online
DOI: 10.1039/D2SE00251E

Oxide	Number of infiltration cycles	Infiltration	Structure	Grains size (nm)
Classical Ni (ICNi1)	15	Homogeneous	Cubic	20 - 170
Supercritical Ni (ISCNi1)	7	Homogeneous	Cubic	40 - 110
Classical Cu (ICCu1)	15	Heterogeneous	Cubic	15 - 50
Supercritical Cu (ISCCu1)	6	Homogeneous	Cubic	≤ 10

3.1. Material characterizations

For the classical infiltration, regarding nickel (ICNi1) and copper (ICCu1), 15 cycles were needed to reach the required 60wt. % of infiltrated metal, therefore corresponding to long experiment times.

For the nickel infiltration assisted by supercritical carbon dioxide, the solution concentration and the solvent nature were the adjusted parameters. By changing the ethanol:water ratio, the solvent wettability as well as its solubility in CO₂ are modified.

Consequently, three samples were prepared:

- (1) the first sample was washed with supercritical CO₂ before infiltration (to remove carbon or other possible contamination), then classically infiltrated with nickel nitrate concentrated at 3 mol.L⁻¹ under primary vacuum. The used solvent was ethanol:water 1:1 (ISCNi1);
- (2) the second sample was infiltrated with the help of supercritical CO₂, using nickel nitrate concentrated at 3 mol.L⁻¹ and ethanol:water 1:3 as solvent (with a vacuum pre-step) (ISCNi2);
- (3) the third sample was infiltrated with the help of supercritical CO₂, using nickel nitrate concentrated at 3 mol.L⁻¹ and ethanol:water 1:3 as solvent (without a vacuum pre-step) (ISCNi3).

In each case, 7 infiltration cycles are necessary to reach the required rate instead of 15 with the conventional infiltration method.

Finally, copper nitrate, with a concentration of 2 mol.L⁻¹ and pure water as solvent, was infiltrated in a GDC backbone by the supercritical way (ISCCu1). Using such method, only 6 cycles were needed to reach an infiltration rate of 60 %wt. of CuO (again instead of 15 with the conventional infiltration method).

3.1.1. Impregnated material nature and cell parameters

XRD analyses were performed on four different samples (ICNi1, ISCNi1, ICCu1 and ISCCu1); the corresponding crystallographic cell parameters are summed-up in Table 2.

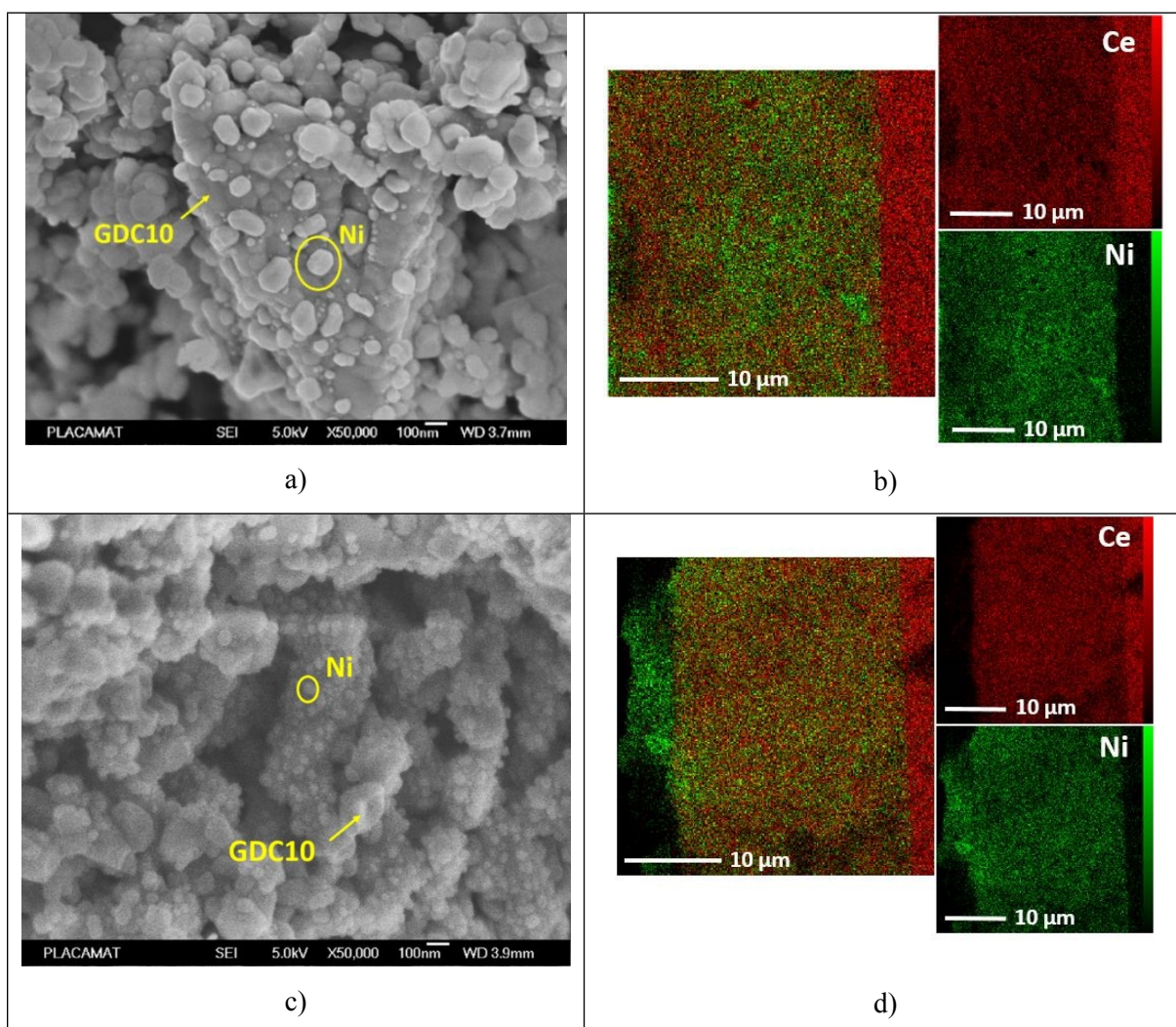
Table 2. Cell parameters (cubic structure) determined on the different infiltrated samples View Article Online
DOI: 10.1039/D2SE00251E

Sample	a (Å)
Classical nickel infiltration (ICNi1)	3,5191
Supercritical nickel infiltration (ISCNi1)	3,5230
Classical copper infiltration (ICCu1)	3,6150
Supercritical copper infiltration (ISCCu1)	3,5970

No major difference between the lattice parameters was observed if comparing the samples infiltrated by classical and supercritical routes (either for nickel and copper). Therefore, the supercritical method has not a major impact on the material crystallographic structure.

3.1.2. Infiltrated material characteristics

The SEM images and EDX analyses recorded according to the different infiltrations processes are gathered on Figure 4.



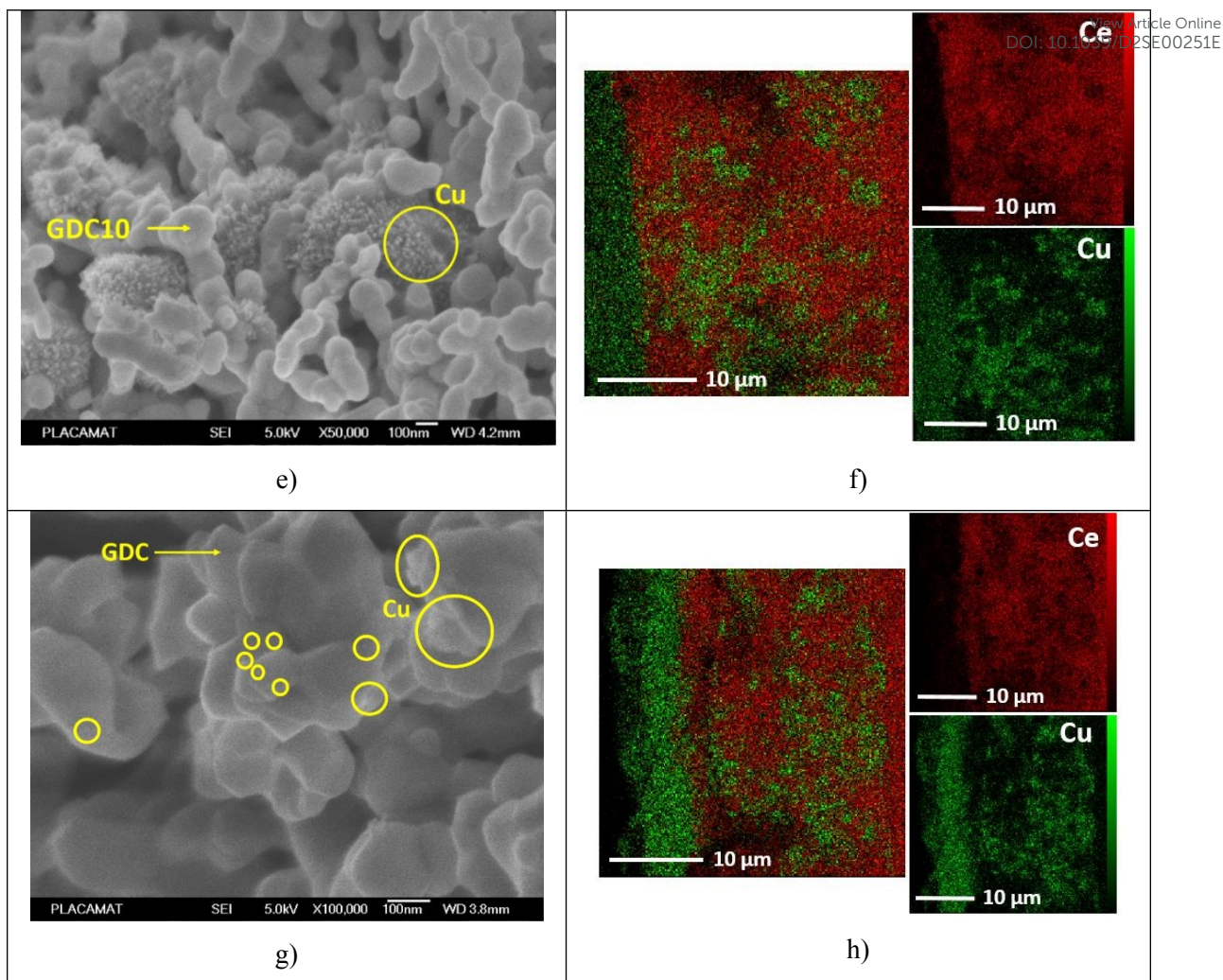


Figure 4. Cross section SEM images and EDS analyses, respectively, recorded on i) GDC-Ni composite anodes prepared by: conventional infiltration (ICNi1) (a and b); infiltration performed in supercritical conditions (ISCNi1) (c and d); ii) GDC-Cu composite anodes prepared by : conventional infiltration (ICCu1) (e and f) ;infiltration performed in supercritical conditions (ISCCu1) (g and h)

In each case, the nanoparticles evidenced on the SEM images correspond to reduced metal particles (Ni and Cu). An example of XRD diagram is given on Figure 5, recorded after the infiltration step, then the annealing performed at 600 °C, under $H_2/3\%H_2O$ gas flow. Please note that the current collector layer was removed prior to the XRD record. Metallic nickel is well evidenced on the XRD diagram, as expected.

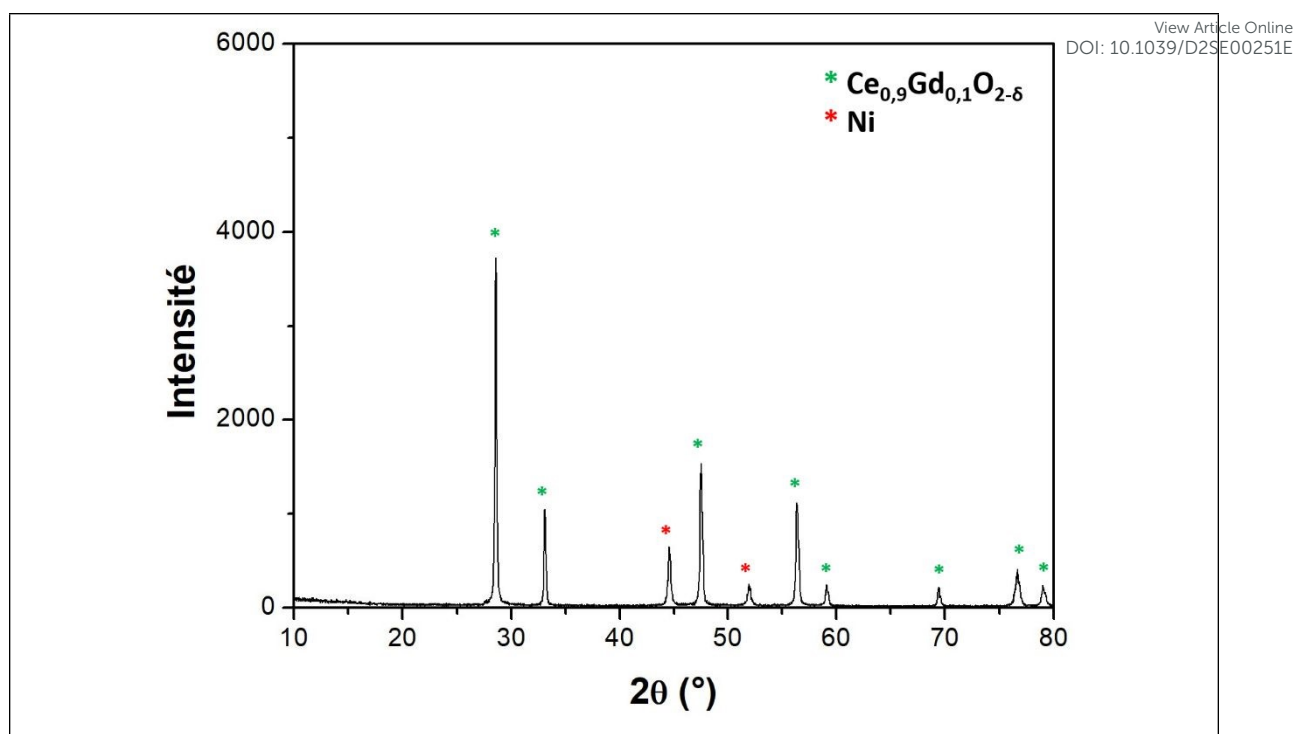


Figure 5 – XRD recorded on the ICNi1 sample, after the reduction step performed at 600 °C, under $\text{H}_2/3\%\text{H}_2\text{O}$ gas flow, and the polishing of the current collector layer

With the help of SEM observations and EDX analyses (Figures 4.a and 4.b), we concluded that the nickel infiltration into a porous GDC skeleton performed by classical way is homogeneous with a nickel grain size between 20 and 170 nm. Due to this homogeneous infiltration, this kind of cells could be efficient in symmetrical configuration. Figures 4.c and 4.d gathered the SEM images and the corresponding EDX analysis recorded on the sample infiltrated with nickel nitrate using the supercritical process. The nickel particle size distribution is narrower when compared to the conventional infiltration (between 40 and 110 nm instead of 20 and 170 nm for the classical infiltration) as shown on Figure 6. On another hand, the homogeneity of the particle infiltration already observed using classical infiltration is kept.

For the copper infiltration, using the classical way the SEM image recorded on this electrode (Figure 4.e) evidences an agglomeration of copper nanoparticles which sizes are between 15 and 50 nm, then smaller compared to that of nickel (Figure 6). The EDX analysis (Figure 4.f) evidenced that the infiltration is heterogeneous. Finally, for the supercritical infiltration of copper (Figures 4.g and 4.h), an improved homogeneity compared to the conventional infiltration is evidenced and the grain size is decreased (less than 10 nm for the supercritical infiltration). In this case, it is difficult to determine the (very low) particles size and their amount, then the size distribution was not included in Figure 6.

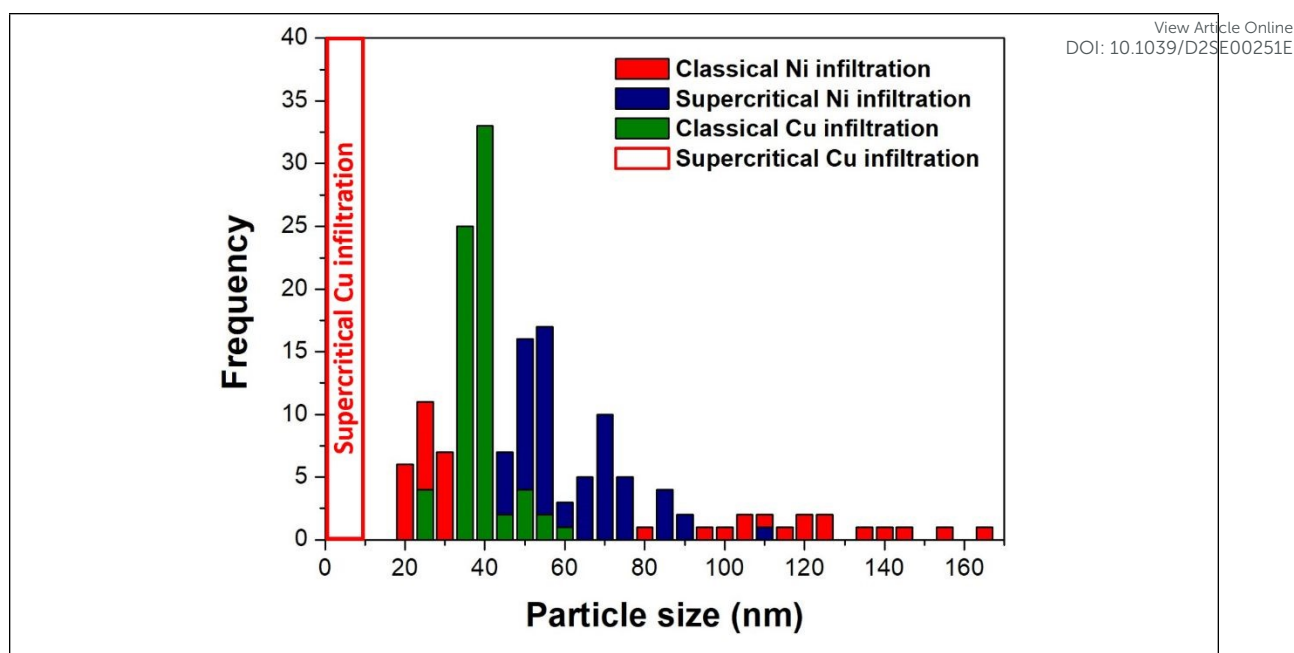


Figure 6. Histograms of the particles size distribution for each infiltration route

To conclude on this part, the supercritical infiltration allows significantly reducing the infiltration cycles number and is especially efficient for the infiltration of copper, which is not really possible with the conventional method.

3.1.3. Discussion

With the help of the Ellingham diagram, when comparing the respective data for CuO and NiO one can conclude that the formation of metallic Cu and Ni is possible, from a thermodynamic point of view, in both cases and in the experimental reducing conditions we used in this work. It is validated by TGA analyses, indeed CuO and NiO oxides are rapidly and fully reduced under H₂ at 600°C, only after about 150 min (see Figure 7).

However, we can not at this stage easily explain the larger size of the obtained metallic nickel particles compared to the copper one, because kinetics factors would have to be taken into account. They can differ in both cases. Moreover, to this purpose it would be necessary to perform a careful SEM images comparison between the infiltrated CuO and NiO particles, obtained after the nitrate annealing, which was not the goal of the present work.

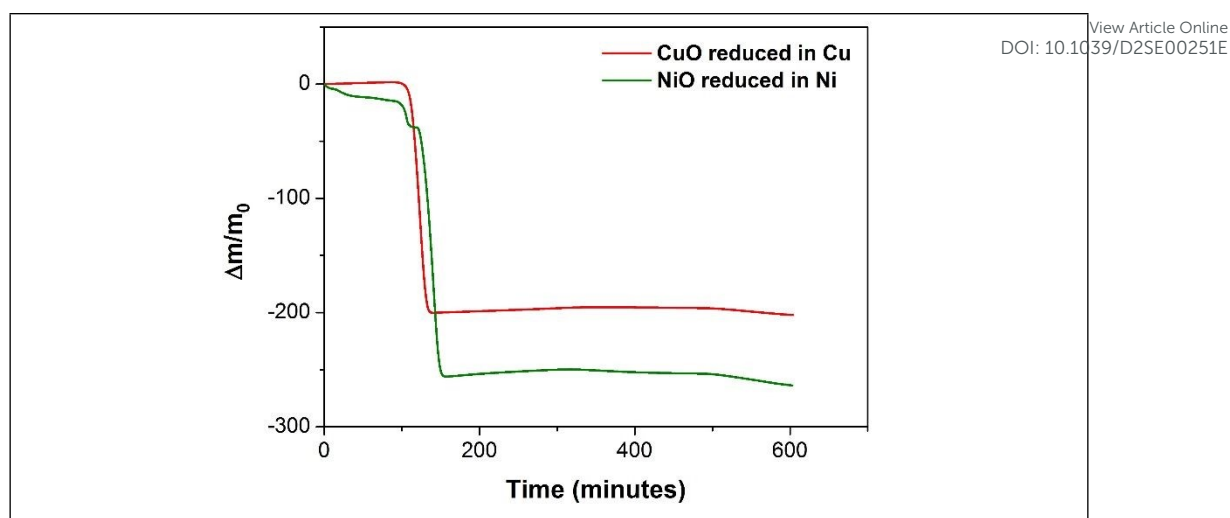


Figure 7. TGA analysis of CuO and NiO under H₂ at 600°C as a function of time

3.2. Electrochemical performances

On Figure 3 are plotted the experimental impedance diagrams recorded on the four studied cells. Then, the evolution of the ratio ΔR_s ($\Delta R_s = R_{s, \text{cell}} - R_{s, \text{ref}}$) / $R_{s, \text{ref}}$ versus temperature, determined on the different studied cells, was plotted in Figure 8.a. The corresponding values at 500 and 600°C (the expected operating temperatures of the cells) are gathered in Table 3.

For all infiltrations, the objective was reached and, at low temperatures, $R_{s, \text{cell}}$ is even lower than $R_{s, \text{ref}}$ (Figure 8.a). We can conclude that i) the electronic conductivity brought by either metallic nickel or copper is sufficient, and ii) the interfaces between the different components of the cells are efficient, because not blocking the transfer of electrons (between the collecting layer and the catalyst) and ions (between the backbone and the electrolyte). In particular, the decoration of the GDC10 backbone with nano-particules of nickel / copper infiltrated by supercritical leads, in our opinion, to a large number of triple point boundaries and an improved oxygen charge transfer.

Table 3. $\Delta R_s / R_{s, \text{ref}}$ values recorded on the nickel and copper infiltrated samples, at 500 and 600°C

Samples	$\Delta R_s / R_{s, \text{ref}}$ at 500°C	$\Delta R_s / R_{s, \text{ref}}$ at 600°C
Classical infiltration of Ni (ICNi1)	-0.21	-0.09
Supercritical infiltration of Ni (1) (ISCNi1)	0.04	0.19
Supercritical infiltration of Ni (2) (ISCNi2)	0.14	0.24
Supercritical infiltration of Ni (3) (ISCNi3)	0.24	0.32
Classical infiltration of Cu (ICCu1)	-0.12	-0.19
Supercritical infiltration of Cu (ISCCu1)	-0.07	-0.10

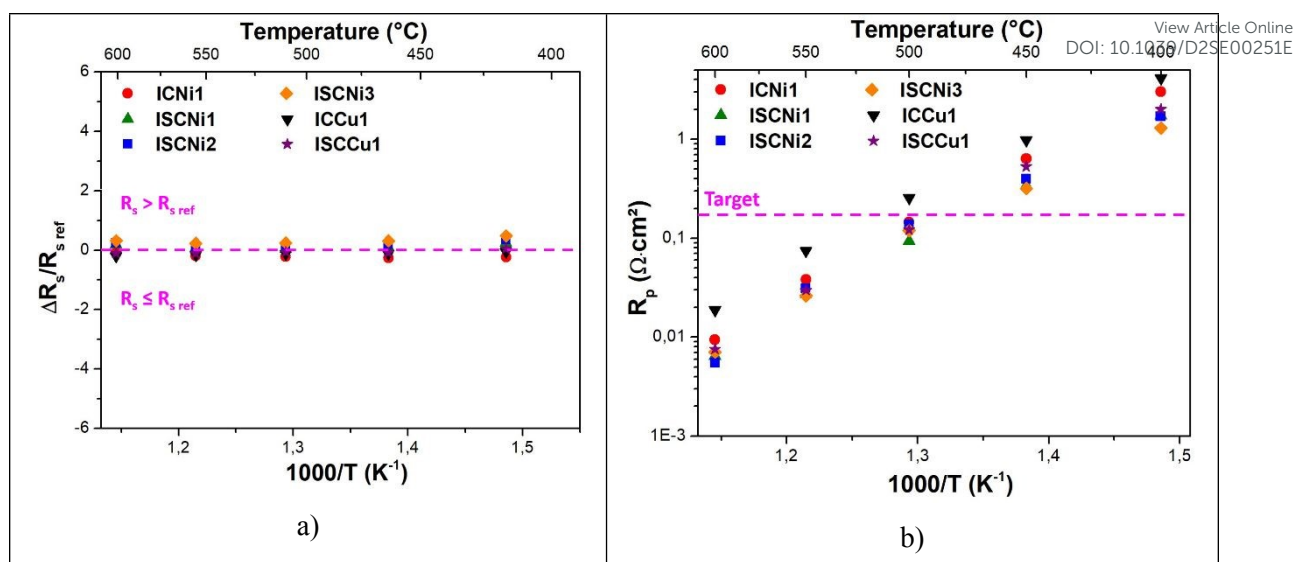


Figure 8. Arrhenius plots of series (a) and polarization (b) resistances measured on symmetrical cells (nickel or copper nitrate infiltration in a porous GDC10 backbone)

For the polarization resistance (Figure 8.b), the objective is to get a R_p value equal or less than $0.15 \Omega \cdot \text{cm}^2$ at the operation temperature, as argued, for instance, by Steele et al. [48].

For the classical nickel infiltration, the R_p values measured are very low: $R_p = 0.009 \Omega \cdot \text{cm}^2$ at 600°C , then a $R_p = 0.15 \Omega \cdot \text{cm}^2$ was obtained at low temperature ($T \sim 500^\circ\text{C}$).

The electrochemical performances of the three samples prepared by the supercritical method for nickel are measured, while the R_p values determined at $T = 500$ and 600°C are gathered in Table 4 for all samples. No major R_p difference is observed between classical and supercritical infiltrations. However, in the second case the experimental process involving nickel nitrate concentrated at $3 \text{ mol} \cdot \text{L}^{-1}$ and ethanol:water 1:3 as solvent, without a vacuum pre-step (ISNi3) seems the most efficient one to improve the polarization resistance. The number of infiltration cycles is about half compared to the infiltration process by classical way, but at the same time this new shaping method permits to obtain a tighter particles size distribution. Moreover, let us indicate that the (composite) electrode has the expected porosity with a well defined interface with the dense electrolyte part.

Finally, whatever the infiltration process (with the same catalyst loading amount), the Ni-based electrode is very efficient. However, the supercritical way enables to largely decrease the number of infiltration cycles, which was the expected goal.

Table 4. R_p values of the nickel infiltrated samples, at 500 and 600°CView Article Online
DOI: 10.1039/D2SE00251E

Samples	R_p at 500°C ($\Omega \cdot \text{cm}^2$)	R_p at 600°C ($\Omega \cdot \text{cm}^2$)
Classical infiltration of Ni (ICNi1)	0.14	0.009
Supercritical infiltration of Ni (1) (ISCNi1)	0.09	0.006
Supercritical infiltration of Ni (2) (ISCNi2)	0.14	0.006
Supercritical infiltration of Ni (3) (ISCNi3)	0.12	0.007

For the copper infiltration by classical way, the R_p values determined on symmetrical infiltrated cells are, again, very low ($R_p \sim 0.02 \Omega \cdot \text{cm}^2$ at 600 °C) as plotted on Figure 8.b. However, the copper infiltrated cell is a bit less efficient, regarding the electrochemical performances, compared to the nickel one: for instance, at 500°C, R_p (ICCu1) = 0.26 $\Omega \cdot \text{cm}^2$ while R_p (ICNi1) = 0.14 $\Omega \cdot \text{cm}^2$. At 500°C, the target R_p (ICCu1) = 0.15 $\Omega \cdot \text{cm}^2$ is reached using the nickel infiltration but not for the copper one.

For the supercritical infiltration, as shown on Figure 8.b and Table 5, the electrochemical performances of the corresponding cell are significantly improved compared to the cell prepared using conventional infiltration. Indeed, the R_p resistance decreased from 0.26 $\Omega \cdot \text{cm}^2$ down to 0.12 $\Omega \cdot \text{cm}^2$ at 500°C (and from 0.019 $\Omega \cdot \text{cm}^2$ down to 0.008 $\Omega \cdot \text{cm}^2$ at 600°C, Table 5). At the same time, again the number of impregnation cycles (in order to reach the same amount of catalyst loading) is divided by two compared to the infiltration by classical way. The corresponding huge decrease of the (un-agglomerated) copper particles size is here involved.

Table 5. R_p values of the copper infiltrated samples, at 500 and 600°C

Samples	R_p at 500°C ($\Omega \cdot \text{cm}^2$)	R_p at 600°C ($\Omega \cdot \text{cm}^2$)
Classical infiltration of Cu (ICCu1)	0.26	0.019
Supercritical infiltration of Cu (ISCCu1)	0.12	0.008

As a partial conclusion, the electrochemical performances are the most improved when involving the supercritical infiltration of copper. Likewise, it is more interesting to use copper instead of nickel, the latter being highly toxic to humans. Moreover, nickel is much more expensive than copper.

3.3. Correlations between the microstructure of the electrodes and their electrochemical performances

We established here a link between the microstructure of the electrodes and their electrochemical performance:

- Between nickel and copper infiltration using classical routes:

The copper particles are agglomerated, there is therefore a limited exchange surface thus affecting the electrochemical performances of the cell. Moreover, the particle sizes of nickel are bigger than that of copper, due to the reduction kinetics: CuO is reduced faster than NiO, so the copper particles are smaller.

- Between nickel infiltration using classical and supercritical routes:

View Article Online
DOI: 10.1039/D2SE00251E

In each case, the infiltration is homogeneous. However, the supercritical conditions leads to get particles less dispersed in size than the classical infiltration. This phenomenon generates a slight improvement of the electrochemical performance and could allow reducing the infiltrated nickel amount.

- Between copper infiltration using classical and supercritical routes:

In this case, the classical infiltration is heterogeneous because of the agglomeration of copper particles.

When involving the supercritical route, the infiltration becomes more homogeneous and the particles are no longer agglomerated, in link with the large decrease of their size. Using this innovative method, the electrochemical performances are drastically improved, the surface exchange being increased. However, further works are still necessary to obtain a fully homogeneous infiltration.

Conclusion

At the present time of the SOC development, it is mandatory to address the ageing anode problems (mainly the nickel agglomeration and its volatilization). A decrease of the operating temperature is a first way to overcome this issue and, in this frame, the shaping of electrodes has to be modified to keep the best performance at lower temperatures.

The infiltration of a catalyst in an ionic backbone, for instance in a gadolinium doped ceria GDC10, was already used to prepare efficient SOC oxygen electrodes [50]. In this work we aim developing the concept to prepare hydrogen electrodes. Two different catalyst precursors were infiltrated in a GDC10 backbone: nickel and copper nitrates, with the goal to obtain, after reduction under hydrogen flow, metallic nickel and copper highly dispersed in the ionic conducting backbone in order to increase the triple point boundaries concentration and then the electrode efficiency. For this purpose we compared in this work two infiltration routes : 1) a « classical » infiltration (of a nitrate solution) into a porous support, and 2) an original way which is the infiltration assisted by supercritical (SC) carbon dioxide. Two catalysts were infiltrated: metallic nickel and copper, obtained after a final thermal treatment of the nitrates performed under Ar/5%H₂ flow.

Using the classical infiltration route, the infiltration cycles number is high (15) for both copper and nickel in order to reach the target (a weight mass ratio of the infiltrated material over the backbone one of 60 wt. % before reduction under hydrogen). Likewise, for the classical infiltration of copper, the infiltration is heterogeneous, that alters the electrochemical performance. Then, CO₂ was selected as the supercritical fluid to assist the infiltration process because it is non-polluting, abundant and its critical coordinates can be easily reached.

Thanks to the infiltration method performed in SC conditions and applied to such porous electrolytes, the infiltration cycles number was largely decreased (by a factor of two for both nickel and copper), it

is the most important positive effect brings by this route. Moreover, the nanoparticle size distribution became narrower in both cases, resulting in improved electrochemical performances : 1) regarding the infiltration of nickel, the best result is obtained when using a nickel nitrate solution concentrated at 3 mol.L⁻¹ and ethanol :water 1 :3 as solvent, without a vacuum pre-step (ISCNi3). In that case $R_p = 0.12 \Omega \cdot \text{cm}^2$ at 500°C compared to $R_p = 0.14 \Omega \cdot \text{cm}^2$ for the classical infiltration route (0.007 / 0.009 $\Omega \cdot \text{cm}^2$ at 600°C); 2) for copper, the infiltration assisted by scCO₂ permits to improve i) the infiltration homogeneity, which was very limited using the conventional infiltration, and ii) at the same time drastically the electrochemical performance ($R_p = 0,12 \Omega \cdot \text{cm}^2$ at 500°C instead of 0,26 $\Omega \cdot \text{cm}^2$ with the conventional infiltration for copper (0.008 / 0.019 $\Omega \cdot \text{cm}^2$ at 600°C). In that case, we used a copper nitrate solution of 2 mol.L⁻¹ and pure water as solvent, Finally, this original shaping method was validated, and the next step is now to integrate it to prepare complete cells to measure them in SOFC and EHT modes.

References

- [1] T. Matsui, R. Kishida, H. Muroyama, et K. Eguchi, « Comparative Study on Performance Stability of Ni–Oxide Cermet Anodes under Humidified Atmospheres in Solid Oxide Fuel Cells », *Journal of the Electrochemical Society*, p. F456-F460, 2012.
- [2] C. Fu, S. H. Chan, Q. Liu, X. Ge, et G. Pasciak, « Fabrication and evaluation of Ni-GDC composite anode prepared by aqueous-based tape casting method for low-temperature solid oxide fuel cell », *International Journal of Hydrogen Energy*, p. 301-307, 2010.
- [3] F. Monaco *et al.*, « Degradation of Ni-YSZ Electrodes in Solid Oxide Cells: Impact of Polarization and Initial Microstructure on the Ni Evolution », *Journal of the Electrochemical Society*, p. F1229-F1242, 2019.
- [4] S. P. Jiang et S. H. Chan, « A review of anode materials development in solid oxide fuel cells », *Journal of Materials Science*, p. 4405-4439, 2004.
- [5] X.-F. Ye, S. R. Wang, Q. Hu, J. Y. Chen, T. L. Wen, et Z. Y. Wen, « Improvement of Cu–CeO₂ anodes for SOFCs running on ethanol fuels », *Solid State Ionics*, p. 276-281, 2009.
- [6] X. Ding, W. Zhu, G. Hua, J. Li, et Z. Chu, « Enhanced oxygen reduction activity on surface-decorated perovskite La_{0,6}Ni_{0,4}FeO₃ cathode for solid oxide fuel cells », *Electrochimica Acta*, p. 204-212, 2015.
- [7] V. Vibhu *et al.*, « Structural characterization of Pr-rich phases in La_{2-x}Pr_xNiO_{4+δ} series using Synchrotron and Neutron Powder Diffraction », *The Royal Society of Chemistry*, p. 266-277, 2019.
- [8] J.-H. Lee *et al.*, « Degradation Mechanism of Oxygen Electrode Under Fuel-Cell and Electrolysis Mode Operations », *ECS Trans.*, vol. 91, n° 1, p. 681-685, 2019.
- [9] N. H. Menzler, D. Sebold, et S. Zischke, « SOC Degradation: Long-Term and Small-Scale Effects », *ECS Transactions*, vol. 91, n° 1, p. 719-729, 2019.
- [10] M. B. Mogensen *et al.*, « Comprehensive Hypotheses for Degradation Mechanisms in Ni-Stabilized Zirconia Electrodes », *ECS Transactions*, vol. 91, n° 1, p. 613-620, 2019.
- [11] F. Monaco *et al.*, « Impact of Microstructure and Polarization on the Degradation of Ni-YSZ Electrode: An Experimental and Modeling Approach », *ECS Transactions*, vol. 91, n° 1, p. 653-664, 2019.
- [12] M. Z. Zhan, R. H. Song, S. B. Lee, et T. H. Lim, « Lifetime Prediction of Anode-Supported Solid Oxide Fuel Cell on the Basis of Individual Components Degradation », *ECS Transactions*, vol. 91, n° 1, p. 621-627, 2019.

- [13] X.-F. Ye, B. Huang, S. R. Wang, Z. R. Wang, L. Xiong, et T. L. Wen, « Preparation and performance of a Cu–CeO₂–ScSZ composite anode for SOFCs running on ethanol fuel », *Journal of Power Sources*, p. 203-209, 2007. View Article Online
DOI: 10.1039/D2SE00251E
- [14] M. Boaro, J. M. Vohs, et R. J. Gorte, « Synthesis of highly porous yttria-stabilized zirconia by tape-casting methods », *Journal of the American Ceramic Society*, p. 395-400, 2003.
- [15] S. Roudeau, « Nouveaux matériaux d'anodes pour piles à combustible SOFC fonctionnant à 700°C », Université de Bordeaux, 2008.
- [16] D. Simwonis, H. Thulen, F. Dias, A. Naoumidis, et D. Stover, « Properties of Ni/YSZ porous cermet for SOFC anode substrates prepared by tape casting and coat-mix process », *Journal of Materials Processing Technology*, p. 107-111, 1999.
- [17] R. J. Gorte et J. M. Vohs, « Novel SOFC anodes for the direct electrochemical oxidation of hydrocarbons », *Journal of Catalysis*, p. 477-486, 2003.
- [18] M. Hubert, J. Laurencin, P. Cloetens, B. Morel, D. Montinaro, et F. Lefebvre-Joud, « Impact of Nickel agglomeration on Solid Oxide Cell operated in fuel cell and electrolysis modes », *Journal of Power Sources*, p. 240-251, 2018.
- [19] E. Lay-Grindler *et al.*, « Degradation study by 3D reconstruction of a nickeleyttria stabilized zirconia cathode after high temperature steam electrolysis operation », *Journal of Power Sources*, p. 927-936, 2014.
- [20] L. Pelegrini, J. Batista Rodrigues Neto, et D. Hotza, « Process and materials improvements on Ni/Cu-YSZ composites towards nanostructured SOFC anode: a review », *Review on advanced materials science*, p. 6-21, 2016.
- [21] A. Faes, A. Hessler-Wyser, D. Presvytes, C. G. Vayenas, et J. Van herle, « Nickel–Zirconia Anode Degradation and Triple Phase Boundary Quantification from Microstructural Analysis », *Fuel cells*, p. 841-851, 2009.
- [22] M. Hubert, « Durability of Solid Oxide Cells: an experimental and modelling investigation based on synchrotron X-ray nano-tomography characterization », Université de Grenoble, 2017.
- [23] A. N. Busawon, D. Sarantaridis, et A. Atkinson, « Ni Infiltration as a Possible Solution to the Redox Problem of SOFC Anodes », *The Electrochemical Society*, p. B186-B189, 2008.
- [24] J. Garcia-Fayos, R. Ruhl, L. Navarrete, H. J. M. Bouwmeester, et J. M. Serra, « Enhancing oxygen permeation through Fe₂NiO₄–Ce_{0.8}Tb_{0.2}O_{2-δ} composite membranes using porous layers activated with Pr₆O₁₁ nanoparticles », *Journal of Materials Chemistry A*, 2017.
- [25] A. Samson, M. Sogaard, R. Knibbe, et N. Bonanos, « High Performance Cathodes for Solid Oxide Fuel Cells Prepared by Infiltration of La_{0.6}Sr_{0.4}CoO_{3-δ} into Gd-Doped Ceria », *Journal of the Electrochemical Society*, p. B650-B659, 2011.
- [26] C. Nicollet *et al.*, « Preparation and characterization of Pr₂NiO_{4+δ} infiltrated into Gd-doped ceria as SOFC cathode », *Journal of Solid State Electrochemical*, p. 2071-2078, 2016.
- [27] Y. Huang, J. M. Vohs, et R. J. Gorte, « SOFC Cathodes Prepared by Infiltration with Various LSM Precursors », *Electrochemical and Solid-States Letters*, p. A237-A240, 2006.
- [28] R. Chiba, H. Aono, et K. Kato, « An SOFC Cathode Infiltrated with Pr₆O₁₁ », *The Electrochemical Society*, p. 1831-1840, 2013.
- [29] E. Dogdibegovic, R. Wang, G. Y. Lau, et M. C. Tucker, « High performance metal-supported solid oxide fuel cells with infiltrated electrodes », *Journal of Power Sources*, p. 91-98, 2019.
- [30] I. Jang, C. Kim, S. Kim, et H. Yoon, « Effect of Gd infiltration on NiO–CeO₂ anode substrates for intermediate- temperature solid oxide fuel cells », *Ceramics International*, p. 9552-9558, 2017.
- [31] X. Yue, A. Arenillas, et J. T. S. Irvine, « Application of infiltrated LSCM–GDC oxide anode in direct carbon/coal fuel cells », *Royal Society of Chemistry*, p. 269-289, 2016.
- [32] V. Sariboga et M. A. Faruk Oksuzomer, « Cu–CeO₂ anodes for solid oxide fuel cells: Determination of infiltration characteristics », *Journal of Alloys and Compounds*, p. 323-331, 2016.
- [33] N. Oishi, A. Atkinson, N. P. Brandon, J. A. Kilner, et B. C. H. Steele, « Fabrication of an Anode-Supported Gadolinium-Doped Ceria Solid Oxide Fuel Cell and Its Operation at 550°C », *Journal of the American Ceramic Society*, p. 1394-1396, 2005.
- [34] M. Kishimoto, Y. Kawakami, Y. Otani, H. Iwai, et H. Yoshida, « Improved controllability of wet infiltration technique for fabrication of solid oxide fuel cell anodes », *Scripta Materialia*, p. 5-8, 2017.

- [35] S. N. Basu, Y. Lu, P. J. Gasper, S. Gopalan, et U. B. Pal, « Enhancing Anodic Catalytic Activity at High Fuel Utilization by Infiltration of Ni Nanoparticles », *The Electrochemical Society*, p. 1397-1405, 2017. Article Online
DOI: 10.1039/D2SE00251E
- [36] M. Lomberg, E. Ruiz-Trejo, G. Offer, et N. P. Brandon, « Characterization of Ni-Infiltrated GDC Electrodes for Solid Oxide Cell Applications », *Journal of the Electrochemical Society*, p. F899-F905, 2014.
- [37] G. Kim *et al.*, « Investigation of the Structural and Catalytic Requirements for High-Performance SOFC Anodes Formed by Infiltration of LSCM », *The Electrochemical Society*, p. B48-B52, 2009.
- [38] S. Jung, C. Lu, H. He, K. Ahn, R. J. Gorte, et J. M. Vohs, « Influence of composition and Cu impregnation method on the performance of Cu/CeO₂ /YSZ SOFC anodes », *Journal of Power Sources*, p. 42-50, 2006.
- [39] C. Aymonier, G. Philippot, A. Erriguible, et S. Marre, « Playing with chemistry in supercritical solvents and the associated technologies for advanced materials by design », *The Journal of Supercritical Fluids*, vol. 134, p. 184-196, 2018.
- [40] S. B. Barim, E. Uzunlar, S. E. Bozbag, et C. Erkey, « Review—Supercritical Deposition: A Powerful Technique for Synthesis of Functional Materials for Electrochemical Energy Conversion and Storage », *Journal of the Electrochemical Society*, 2020.
- [41] M. Türk et C. Erkey, « Synthesis of supported nanoparticles in supercritical fluids by supercritical fluid reactive deposition: Current state, further perspectives and needs », *The Journal of Supercritical Fluids*, p. 176-183, 2018.
- [42] L. Guesnet, J.M. Bassat, J.C. Grenier, T. Chartier and P.M. Geffroy, « Shaping of ceria-based single solid oxide cells combining tape-casting, screen-printing and infiltration », *Journal of the European Ceramic Society*, vol. 40, p. 5662-5669, 2020.
- [43] K. Tamm, R. Kungas, R. J. Gorte, et E. Lust, « Solid oxide fuel cell anodes prepared by infiltration of strontium doped lanthanum vanadate into doped ceria electrolyte », *Electrochimica Acta*, p. 398-405, 2013.
- [44] S. Lee, G. Kim, J. M. Vohs, et R. J. Gorte, « SOFC Anodes Based on Infiltration of La_{0.3}Sr_{0.7}TiO₃ », *The Electrochemical Society*, p. B1179-B1183, 2008.
- [45] B. Mirfakhraei, S. Paulson, V. Thangadurai, et V. Birss, « Enhanced hydrogen oxidation activity and H₂S tolerance of Ni-infiltrated ceria solid oxide fuel cell anodes », *Journal of Power Sources*, p. 95-101, 2013.
- [46] C. Quilfen, « Supercritical fluids synthesis, characterization and test of HDS catalysts : Assessment of criticality of metals contained in HDS catalysts », Université de Bordeaux, 2016.
- [47] A. Baiker, « Supercritical Fluids in Heterogeneous Catalysis », *Chemical Reviews*, p. 453-473, 1999.
- [48] B. C. H. Steele et A. Heinzl, « Materials for fuel-cell technologies », *Nature*, p. 345-352, 2001.
- [49] S. Park, J. M. Vohs, et R. J. Gorte, « Direct oxidation of hydrocarbons in a solid-oxide fuel cell », *Nature*, vol. 404, p. 265-267, 2000.
- [50] C. Nicollet, A. Flura, V. Vibhu, A. Rougier, J.-M. Bassat, et J.-C. Grenier, « An innovative efficient oxygen electrode for SOFC: Pr₆O₁₁ infiltrated into Gd-doped ceria backbone », *International Journal of Hydrogen Energy*, p. 15538-15544, 2016.